A damage-based temperature-dependent model for ductile fracture with finite strains and configurational forces

N. Van Goethem and P. Areias

June 8, 2012

Abstract

In this paper we assess a crack propagation criterion based on the notion of configurational force in the spirit of Gurtin [26]. We extend the theory of Gurtin to finite strain elasto-plastic fracture and in addition take thermal effects into account. The global model is a system of nonlinear and non-smooth equations which are solved directly with a finite element discretization. Comparison with laboratory experiments is provided, thereby showing that the concept of configurational force can be successfully used for computational damage-based fracture tests on ductile materials.

1 Introduction

Damage [32] and fracture [13] are almost always intimately linked together in the available models for crack propagation coexisting in the literature. For instance, in [1] a damage model is shown to provide crack-like results in some limit case while in [17] (see also [12]) a purely fracture-dedicated theoretical model is implemented numerically with help of an auxiliary variable which has the effect of smearing the crack. In principle, damage must be understood as an internal (here, scalar) thermodynamical variable ζ, which is therefore not necessarily measurable but whose interaction with other mechanical and/or defect variables has visible effects. In the present model, damage is rather a model parameter determining when crack will propagate: at a certain threshold the damage value is such that softening of the material is unbearable without propagation of the crack tip. Let us remark that damage can be cast within purely elastic brittle fracture models but also plays a crucial role in the models designed for ductile materials such as metals, cf. [14] or [2, 40, 51]. In fact, ductile fracture mechanisms under mixed mode I/II load show either shear, or microvoid coalescence behaviors [36], with the latter here modeled by the introduction of ζ.

In most metals, ductile fracture is an elasto-plastic process [28, 34, 39, 51]. Plastic effects are classically understood as a state of the body where external loading and/or thermal fluxes have created residual stresses and irreversible deformations of the metal. As induced and enhanced by mutual interaction of point defects and dislocations, plastic effects are, as damage, particularly observed in a region around the crack tip called the process zone. These effects are localised along the so-called flow tensor $\mathcal{N}$ which is the derivative of the yield function with respect to the Kirchhoff stress tensor. In order to avoid singular points on the yield surface where $\mathcal{N}$ is undefined (thence belonging to a normal cone), multisurface plasticity is here considered [7, 29].

The present model is applied to metal plasticity which is known to produce higher plastic than elastic deformations. Nevertheless, finite strain elasto-plasticity [16, 42] will be considered with a multiplicative decomposition of the deformation tensor [31]. Numerical simulations will be performed with the SIMPLAS code [4] as based on a series previously published contributions [6–8,11]. Triangular finite elements without tip mesh refinement are used with remeshing performed at every iteration to allow crack propagation. Moreover, the flow law is solved directly, i.e., without appealing to return-map algorithms [45], by smoothing the complementarity conditions [19].

Obviously, dissipation phenomena are observed at the crack tip, and hence any realistic model should incorporate the temperature (T) as a thermodynamic variable, besides the left Cauchy-Green tensor. In the present model, the energy equation (with a heat source depending on the plastic dissipation) is solved as coupled to the momentum equation, while the yield functions also depend on T. A first series of ductile crack propagation results with such a temperature-dependence have been

performed and discussed in [49] from which the present contribution has followed. However as opposed to the present model the crack propagation direction was calculated with an empirical law based on a CTOD[1] criterion [35] which is known to provide excellent qualitative results for both brittle and ductile fracture (c.f., e.g., [6, 11, 47]).

Here we propose a model where the direction of crack propagation follows from rational mechanics arguments from Gurtin's theory of configurational forces [26]. The so-called tip traction is calculated as the limit of a contour integral around the crack tip as the contour converges to the tip. For homogeneous elastic bodies, the tip traction is known to be independent of the chosen contour and corresponds to the notion of J-integral [46]. However Gurtin's concepts are formulated in such a way that extension to finite strain elasto-plasticity and incorporation of temperature-dependent laws is easily tractable [25]. Moreover fracture criteria based on the J-integral are known to be geometry-dependent, whereas Gurtin's energy release rate is a purely material criterion.

Our intention in this paper is to show that such a rational fracture criterion (remark that crack tip velocity is also provided) is able to provide remarkable results for two classical benchmark cases, the mode I and mode II crack propagation. Moreover mixed-mode experimental results as reported by M.A. Sutton et al. [47] have been reproduced by our model with good agreement. To conclude the series of numerical simulations, a force-free crack propagation is also shown as an application of the model. Here fracture is driven by the sole heat flux. Note that as opposed to other approaches as based on configurational forces, no tip refinement is required and the contour integral is computed directly (i.e., is not turned into a surface integral by Green's theorem).

Let us emphasize that the present model is based on the so-called Hill-Mandel principle of maximal dissipation [37]. First, the plastic flow law follows from the principle of maximal plastic dissipation [22, 43, 44]. In addition, the kinking angle is also a consequence of this principle as applied to crack tip dissipation with appropriate constitutive relations [26]. Let us also remark that as based on this principle it is also possible to theoretically justify crack nucleation criteria for brittle fracture [50] whereas nucleation of ductile bodies is to the knowledge of the authors not addressed much in the literature from a theoretical viewpoint. We also leave numerical experiences of crack nucleation with this model for future works, and hence the shown examples here are all given with an initial notch. To conclude, let us recall that for ductile fracture the crack tip singularities are less severe than for brittle cracks, and hence the difficulty to deal with in the present model are rather towards the complexity of the global system to solve numerically, which is both nonlinear and nonsmooth.

2 The fracture model

2.1 On the concept of configurational force

Gurtin [26] believes that besides the Newtonian force system, the "configurational forces should be viewed as basic objects consistent with their own force balance". Since a body is free to move in its current configuration by the action of the Newtonian forces, whereas it is not free to move in its reference configuration, Gurtin justifies the existence of internal, *material forces* as those that "pin, in place, the material points of the body, thereby maintaining its internal structure".

These notions are rather abstract, requiring to take some distance from our intuition about forces, while conferring to the force the status of a mathematical concept. Moreover, the balance laws of configurational forces follow from rational thermodynamic arguments such as invariance with respect to change in the *material* observer as the exact analogue of Newtonian laws as derived from invariance principles with respect to change in the *spatial* observer. Moreover Gurtin introduces the counterpart of a control volume in the current configuration, called the *material control volume* $P(t)$ that migrates through the reference body and invokes a nonclassical version of the second law requiring that

$$\frac{d}{dt}\left\{\texttt{free energy of } P(t)\right\} \leq \left\{\texttt{rate at which work is performed on } P(t)\right\}.$$

In [26], these concepts are also specifically developed to study the propagation of a crack.

Let us give a recent interpretation of configurational forces by Gupta & Markenscoff [24], which is illuminating, since it states the *equivalence* between the classical balance laws (i.e., of Newtonian

[1] Crack Tip Opening Displacement

forces) and the work done by the configurational forces: the aforementioned authors prove that the energy release (associated with the configurational force) "ensures that the body remains infinitesimally close to equilibrium even after a small perturbation of the inhomogeneity position." A further refinement of their approach can be found in [23, 33].

2.2 Preliminary results for the model

Let us assume the multiplicative decomposition of the deformation tensor $\mathbf{F}$, i.e., the existence of a local plastic process associated to a local reference configuration and a plastic deformation $\mathbf{F^p}$ such that

$$\mathbf{F} = \mathbf{F^e}\mathbf{F^p}, \tag{2.1}$$

where $\mathbf{F^e}$ defines the elastic deformation [31, 48].

Definition 1 *The free energy is a function $\hat{\Psi}$ of the left Cauchy-Green tensor $\mathbf{b^e} := \mathbf{F^e}\mathbf{F^{e}}^T$ and of the temperature T:*

$$\Psi(X,t) = \tilde{\Psi}(\mathbf{F}(X,t), \mathbf{F^p}(X,t), T(X,t); \zeta(X,t)) = \hat{\Psi}(\mathbf{b^e}(X,t), T(X,t)), \tag{2.2}$$

with an implicit dependence on the auxiliary (scalar, internal) variable ζ which represents damage.

Note that the free energy does not depend explicitly on the damage coefficient, but $\mathbf{b^e}$ depends on ζ through the yield function dependence on ζ and the flow rules (cf. §3.2 for detail). Let us remark that the material inhomogeneity is due to temperature-dependence of the free energy but also provoked by the assumed non-vanishing plastic deformations $\mathbf{F^p}$, in such a way that $\mathbf{b^e} \neq \mathbf{F}\mathbf{F}^T$.

Let Ω denote the reference body and $[0, t^\star]$ be the interval of time where the evolution of a crack will be considered. We intend to analyze and perform numerical simulations of ductile fracture, a representation of which is shown in Figure 1.

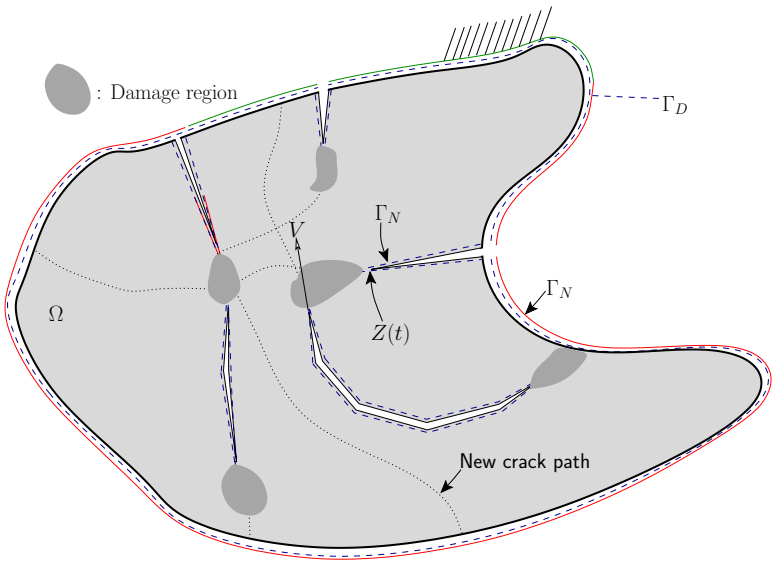

Figure 1: Ductile fracture in the deformed configuration.

Let t be the current time and $\boldsymbol{Z}(t) \in \Omega$ denote the crack tip. Moreover, following Gurtin [26] $D_\delta(t)$ designates the disk centered and of radius $\delta > 0$, $P(t)$ a so-called "tip control volume", and $P_\delta(t) = P(t) \setminus D_\delta(t)$ be a family of bulk control volumes converging to P.

Definition 2 (Tip integrals) *Recalling Figure 2, the following tip integrals are defined*

$$\begin{aligned} \oint_{tip} h dL &= \lim_{\delta \to 0} \oint_{\partial D_\delta} h dL \\ \int_{tip} H dS &= \lim_{\delta \to 0} \int_{D_\delta} H dS, \end{aligned}$$

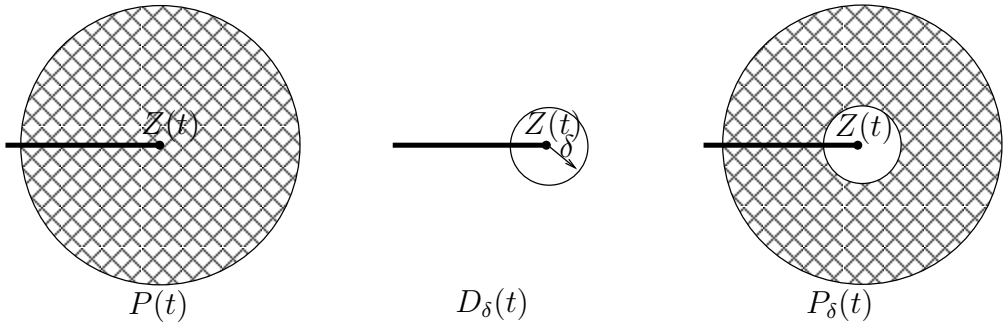

Figure 2: The notions of crack control volume P, the crack tip disk D_δ and the definition of P_δ.

where the functions h and H have appropriate regularity.

Definition 3 (Time derivative following ∂P) *Let $\boldsymbol{q}$ be a velocity field for the particle labeled by $\boldsymbol{X} \in \partial P(t)$. Its trajectory $\boldsymbol{\chi}(\tau)$ $(t \le \tau \le t^\star)$ is defined as the solution of $\dot{\boldsymbol{\chi}}(\tau) = \boldsymbol{q}(\boldsymbol{\chi}(\tau), \tau)$ with $\boldsymbol{\chi}(t) = \boldsymbol{X}$.*

The time derivative of a field Ψ following ∂P is defined as

$$\overset{\circ}{\Psi}(\boldsymbol{X}, t) := \frac{d}{d\tau}\Psi(\boldsymbol{Z}(\tau), \tau)_{|\tau=t}. \tag{2.3}$$

Since they serve as basis of our model, we here recall the three following assumption, lemma and definition which are also proved and discussed in [26].

Assumption 1 (Regular free energy) *Let us assume that the free energy Ψ is smooth away from the tip and that its integral and the integral of its material derivative over P exist in terms of their Cauchy principal value, i.e.,*

$$\int_P \Psi dS := \lim_{\delta\to 0}\int_{P_\delta} \Psi dS < \infty \quad \textit{and} \quad \int_P \overset{\circ}{\Psi}\, dS := \lim_{\delta\to 0}\int_{P_\delta} \overset{\circ}{\Psi}\, dS < \infty. \tag{2.4}$$

Lemma 1 *Under Assumption 1, it holds, uniformly in time:*

$$\lim_{\delta\to 0}\int_{D_\delta} \Psi dS = 0 \quad \textit{and} \quad \lim_{\delta\to 0}\frac{d}{dt}\int_{D_\delta} \Psi dS = 0. \tag{2.5}$$

Let $\mathbf{N}$ be the exterior unit normal to $\partial D_\delta(t)$ and $\mathbf{T}$ be the crack direction at time t.

Definition 4 *By Lemma 1 and in the absence of bulk forces and surface tension on the crack, the dissipation at the crack tip is defined as*

$$\Gamma_{tip} := \oint_{tip} (\mathbf{P}\mathbf{N}\cdot\dot{\mathbf{y}} + V\mathbf{N}\cdot\mathbf{T}\Psi)\, dL, \tag{2.6}$$

where $\mathbf{y}(\boldsymbol{X})$ is the position of material point $\boldsymbol{X}$ in the deformed configuration and $\dot{\mathbf{y}}(X,t)$ the motion velocity of $\boldsymbol{X}$. Moreover, V is the crack tip speed, $\mathbf{P}$ the first Piola-Kirchhoff stress[2], and $\mathbf{N}$ the unit external unit normal to the contour.

2.3 Configurational forces with finite elastoplastic strains

In contrast with Gurtin, we do not require that the internal configurational force $\mathbf{g}$ be integrable in the sense of Cauchy (cf. Assumption 1). In fact be believe that this condition is too restrictive and in particular does not allow for concentration properties at the crack tip. We believe that the notion of Radon measure is much more appropriate in view of the Radon-Nykodým (or Lebesgue)

[2]equivalent to Cauchy stress for small strains.

decomposition (cf., e.g., [38]) of such a measure in a diffuse regular part and in a singular part which we here assume to be purely concentrated. Moreover, a measure is by definition an *extensive* field, and this property is required to confer to $\mathbf{g}$ the interpretation of a force: both the regular integrable and the concentrated parts are extensive fields, whereby all non-measure concentrated distributions are excluded as tip forces.

Assumption 2 *The internal body force* $\mathbf{g}$ *is assumed to be finite Radon measure on* Ω*, whose singular part is purely concentrated at* $\boldsymbol{Z}$*, that is, by Radon-Nykodým decomposition,*

$$\mathbf{g} = \tilde{\mathbf{g}} + \mathbf{g}^\star \delta_{\boldsymbol{Z}} \tag{2.7}$$

with $\tilde{\mathbf{g}}$ *Lebesgue-integrable on* Ω*.*

It should however be precised that for the purpose of the present work, $\mathbf{g}$ could have been chosen Lebesgue-integrable only, i.e., without allowing for a concentrated body force contribution. The choice of assuming $\mathbf{g}$ as a measure is made because, on the one hand, it does not renders the forthcoming exposition more complicated, and on the other hand because from a physical viewpoint, there exists situations where concentrated forces must be accounted for, as for instance as soon as dislocations are present.

The following Result is a straightforward extension of a result of Gurtin [26].

Lemma 2 (Balance laws) *For any tip control volume* D*, the standard and configurational force balances and the second Law entail* [3]

$$\int_{\partial D} \mathbf{P}\mathbf{N}\, dL = 0 \tag{2.8}$$

$$\int_{\partial D} \left(\Psi \mathbf{I} - \mathbf{F}^T\mathbf{P}\right)\mathbf{N}\, dL + \int_D \mathbf{g} dS + \mathbf{g}_{tip} = 0, \tag{2.9}$$

where $\mathbf{g}_{tip}$ *is Gurtin's internal configurational force. Then,*

$$\text{Div } \mathbf{P} = 0 \quad \textit{and} \quad \mathbf{g} + \text{Div } \mathbf{C} = -\mathbf{g}_{tip}\delta_{\boldsymbol{Z}} \quad \textit{with} \quad \mathbf{C} := \Psi I - \mathbf{F}^T\mathbf{P}, \tag{2.10}$$

and where Div *is a symbol recalling the distributional nature of the divergence.*

Note that in component form $\mathbf{g} + \mathbf{g}_{tip}\delta_{\boldsymbol{Z}} = -\text{Div } \mathbf{C}$ writes by (2.8) and (2.10) as[4]

$$\begin{aligned} \tilde{g}_i + (g^\star + g_{tip})_i \delta_{\boldsymbol{Z}} &= -D_j C_{ij} = -D_j\left(\Psi\delta_{ij} - F_{ki}P_{kj}\right) \\ &= -D_i\Psi + D_j\left(F_{ki}P_{kj}\right) = s\partial_i T - \Sigma^e_{kl} D_i b^e_{kl} + P_{kj} D_j F_{ki}, \end{aligned} \tag{2.11}$$

where D_i denotes the distributional derivative, and where we have defined the *plastic thermodynamic stress* and the *entropy* as

PLASTIC THERMODYNAMIC STRESS: $$\boldsymbol{\Sigma}^{\mathbf{e}} := \frac{\partial \hat{\Psi}}{\partial \mathbf{b}^{\mathbf{e}}} = \frac{1}{2}\mathbf{P}\mathbf{F}^T\mathbf{b}^{\mathbf{e}-1} \tag{2.12}$$

ENTROPY: $$s := -\frac{\partial \hat{\Psi}}{\partial T}. \tag{2.13}$$

Let us remark that the bulk configurational force $\tilde{\mathbf{g}} \in L^1(\Omega)$, which is the regular part of $\mathbf{g}$, is by definition less regular than Ψ. In fact, Eqs. (2.4) and (2.5) do not hold for $\tilde{\mathbf{g}}$, since the integral of $\tilde{\mathbf{g}}$ over D_δ in (2.9) must not vanish as $\delta \to 0$. Nevertheless, in view of Eqs. (2.4) and (2.5) it is still assumed that (cf. Assumption 1 with P replaced by D_δ),

$$\lim_{\delta\to 0} \int_{D_\delta} s\nabla T\, dS = 0. \tag{2.14}$$

[3] We write $\mathcal{G} := \int_D \mathbf{g} dS$ with an abuse of notations. It should be written $\mathcal{G} = \int_D d\mathbf{g}$ with $d\mathbf{g}$ the density of measure $\mathbf{g}$, i.e., $\mathcal{G} = \int_D \tilde{\mathbf{g}} dS + \mathbf{g}^\star(\boldsymbol{Z})$.

[4] Here $\text{Div } \mathbf{C} = \mathbf{C}\cdot\nabla + (\text{Div } \mathbf{C})_{\llcorner \boldsymbol{Z}}$ is a measure where we have componentwise, following Gurtin's convention, $(\text{Div } \mathbf{C})_j = D_j C_{ij}$, with the regular part $(\mathbf{C}\cdot\nabla)_j = \partial_j C_{ij}$ and the concentrated part $(\text{Div } \mathbf{C})_{\llcorner \boldsymbol{Z}}$.

By (2.8)-(2.14) and recalling the definitioon of D_δ on Figure 2, we further entail that for every $\delta > 0$,

$$\tilde{\mathbf{g}} := -\mathbf{C}\cdot\nabla \quad \text{a.e. in} \quad D_\delta \setminus \{\boldsymbol{Z}\} \tag{2.15}$$

$$(\mathbf{g}^\star + \mathbf{g}_{tip})\,\delta_{\boldsymbol{Z}} := -\lim_{\delta\to 0}\int_{D_\delta} \text{Div } \mathbf{C}\; dS \quad \text{at} \quad \boldsymbol{Z} \tag{2.16}$$

Since $\mathbf{C}\cdot\nabla \in L^1(D_\delta)$, Eq. (2.9) can be rewritten with D replaced by D_δ,

$$\int_{\partial D_\delta} \mathbf{CN}\; dL - \int_{D_\delta} (\mathbf{C}\cdot\nabla)\, dS = -\left(\mathbf{g}_{tip} + \mathbf{g}^\star\right), \tag{2.17}$$

for every $\delta > 0$.

As a consequence, recalling (2.11) and Definition 2, and letting $\delta \to 0$, the crack tip tractions are introduced as follows.

Definition 5 (Crack tip tractions)

$$\mathbf{j}^{\mathbf{e}} := \oint_{tip} \left(\Psi\mathbf{I} - \mathbf{F}^T\mathbf{P}\right)\mathbf{N}\; dL \tag{2.18}$$

$$\mathbf{j}^{\mathbf{p}} := -\int_{tip} (\boldsymbol{\Sigma}^{\mathbf{e}} \colon \mathbf{b}^{\mathbf{e}}\nabla - \mathbf{P} \colon \nabla\mathbf{F})\, dS \tag{2.19}$$

$$\mathbf{j} := \mathbf{j}^{\mathbf{p}} + \mathbf{j}^{\mathbf{e}} = -\left(\mathbf{g}_{tip} + \mathbf{g}^\star\right) \quad \textit{and} \quad \mathbf{i} := \frac{\mathbf{j}}{\|\mathbf{j}\|}. \tag{2.20}$$

Remark that we have here extended Gibbs notation to operators and tensors whereby according to the notation $\mathbf{A}\colon\mathbf{B} = A_{ij}B_{ji}$ one has $(\boldsymbol{\Sigma}^{\mathbf{e}} \colon \mathbf{b}^{\mathbf{e}}\nabla)_k = \Sigma^e_{ij}\dfrac{\partial b^e_{ji}}{\partial X_k} = \Sigma^e_{ij}\dfrac{\partial b^e_{ij}}{\partial X_k}$ and $(\mathbf{P}\colon\nabla\mathbf{F})_k = P_{ij}\partial_j F_{ik}$.

The following assumption of physical nature will be made in this paper. It will be validaded by comparing the norms of $\mathbf{j}^{\mathbf{e}}$ and $\mathbf{j}^{\mathbf{p}}$ for one of the selected examples in §5.3, Fig. 17.

Assumption 3 (Limited plasticity) *Plastic*[5] *effects are assumed limited in the sense that* $\mathbf{j}^{\mathbf{p}}$ *is negligible with respect to* $\mathbf{j}^{\mathbf{e}}$.

The physical Assumption 3 can be replaced by the following mathematical one.

Assumption 4 (Regular internal body force) *Either the internal body force* $\mathbf{g}$ *is square integrable on* Ω*, or the following holds true:*

$$\int_P \mathbf{g}\; dS := \lim_{\delta\to 0}\int_{P_\delta} \mathbf{g}\; dS < \infty, \tag{2.21}$$

with the notations of Figure 2.

The following Lemma states their equivalence.

Lemma 3 *Under Assumption 4,* $\mathbf{j}^{\mathbf{p}} = 0$.

Proof. If $\mathbf{g} \in L^2(\Omega)$ then $|\int_{D_\delta} \mathbf{g}dS| \le c\delta\|\mathbf{g}\|_{L^2(\Omega)} \to 0$ as $\delta \to 0$. If (2.21) holds the claim is proved by Lemma 1. In both cases, (2.9) rewrites as

$$\lim_{\delta\to 0}\int_{\partial D_\delta} \left(\Psi\mathbf{I} - \mathbf{F}^T\mathbf{P}\right)\mathbf{N}dL = -\mathbf{g}_{tip}, \tag{2.22}$$

and the proof is achieved by (2.18)-(2.20), since $\mathbf{g}^\star = 0$. □

[5]Here subscripts e and p stand for convenience for "elastic" and "plastic". However plastic effects are of course taken into account in $\mathbf{j}^{\mathbf{e}}$ which depends on Ψ.

In physical terms Assumption 4 means that the internal body force is smooth enough. In particular, if dislocations, whose stress distribution is known to be singular, are emitted from the crack tip, then neither $\mathbf{g}$ will satisfy (2.21), nor it will be square integrable, and $\mathbf{j^P}$ can not be neglected.

Assuming that either Assumption 3 or 4 holds, we now introduce the classical definition of energy release rate, which will suffice for the application purposes of the present work.

Definition 6 (Energy release rate)

$$f^e \quad := \quad \mathbf{j^e} \cdot \mathbf{T}, \tag{2.23}$$

where $\mathbf{T}$ *is the crack direction.*

The following Lemma can also be found in [26].

Lemma 4 (Dissipation) *The second law and the balance of configurational forces entail*

$$\Gamma_{tip} = f^e V \geq 0, \tag{2.24}$$

with $V, f^e \geq 0$.

Corollary 1 (Crack tip speed) *It follows from* (2.6) *and* (2.24) *that*

$$V = \left\langle \frac{P^*_{tip}}{f^*} \right\rangle_+ \tag{2.25}$$

with $P^*_{tip} := \oint_{tip} (\mathbf{PN}) \cdot \dot{\mathbf{y}} dL$ *and* $f^* := -\oint_{tip} \left(\mathbf{F}^T\mathbf{P}\right) \cdot (\mathbf{T} \otimes \mathbf{N})\, dL$, *while* $\langle\cdot\rangle_+$ *denotes the "plus" function defined as* $\langle x\rangle_+ = \max\{x, 0\}$.

Proof. From (2.6), (2.24) and (2.23),

$$V \oint_{tip} \left(\Psi\mathbf{I} - \mathbf{F}^T\mathbf{P}\right) \mathbf{N} dL \cdot \mathbf{T} = \oint_{tip} (\mathbf{PN}) \cdot \dot{\mathbf{y}} dL + V \oint_{tip} (\Psi\mathbf{I}) \cdot (\mathbf{N} \otimes \mathbf{T})\, dL,$$

from which (2.25) follows with the positive part $\langle\cdot\rangle_+$ taken because V is assumed nonnegative. □

2.4 Dissipation at the crack tip and kinking

The following statement is taken from Gurtin [26].

Assumption 5 (Constitutive assumptions) *Let* θ *be the kinking angle at time* t, *i.e. the crack is assumed to propagate in a direction forming a counter-clockwise angle* θ *with* $\mathbf{T}$, *i.e.* $\mathbf{T} = \hat{\mathbf{T}}(\theta)$, *with* $\boldsymbol{n} = \mathbf{T}' = \hat{\boldsymbol{n}}(\theta)$, *the normal to the crack. It is assumed that*

$$f^e = \hat{f}^e(\theta) = \mathbf{j}^e \cdot \hat{\mathbf{T}}(\theta), \tag{2.26}$$

with $\mathbf{j}^e$ *as defined by* (2.18) *independent of* θ. *Moreover, the tip speed* V *is assumed isotropic, i.e.,* $V = \hat{V}(f^e)$, *and satisfying*

$$V, V', V'' > 0 \quad \textit{if} \quad f^e \geq f^e_{crit} > 0. \tag{2.27}$$

Then, Eq. (2.24) and Assumption 5 yield $\Gamma_{tip}(\theta) = f^e(\theta)\hat{V}(\hat{f}^e(\theta))$ with

$$\Gamma'_{tip}(\theta) \quad = \quad (f^e)'(V' f^e + V) \tag{2.28}$$

$$\Gamma''_{tip}(\theta) \quad = \quad (f^e)''(V' f^e + V) + ((f^e)')^2(V'' f^e + 2V') \tag{2.29}$$

where, by (2.26),

$$(f^e)' = \mathbf{j}^e \cdot \hat{\mathbf{N}}(\theta) \quad \text{and} \quad (f^e)'' = -f^e. \tag{2.30}$$

In classical fracture mechanics, the principle of maximal dissipation is often postulated [37]. It also our approach to follow Gurtin with this respect, thereby assuming this principle, whose major consequence is to determine the crack propagation direction $\hat{\mathbf{T}}(\theta^{MAX})$ as parallel to the elastic tip traction.

Law 1 (Maximal dissipation) *The internal variables are such that at every time t, the dissipation* Γ_{tip} *is maximized at the crack tip.*

Theorem 1 (Crack propagation direction) *Assume that the crack kinks at time t along a direction* $\hat{\mathbf{T}}$ *forming a counter-clockwise angle* θ^{MAX} *with its orientation at time t in order to maximize the dissipation* Γ_{tip} *at* θ^{MAX}*. Then,*

$$\mathbf{i} = \frac{\mathbf{j}^e}{\|\mathbf{j}^e(t)\|} = \hat{\mathbf{T}}(\theta^{MAX}), \tag{2.31}$$

with $\mathbf{j}^e$ *given by* (2.18)*.*

Proof. From (2.29), the critical states of the dissipation are given by

$$\theta \quad \in \quad \Theta^e := \{(f^e)' = 0\} \quad \text{if} \quad V' \geq 0. \tag{2.32}$$

Moreover at critical points the dissipation is maximized, since

$$\Gamma''_{tip}(\Theta^e) \quad = \quad -f^e(V'f + V) < 0. \tag{2.33}$$

As a consequence, the kinking angle maximizing the tip dissipation is $\theta^{MAX} \in \Theta^e$ such that $(f^e)'(\theta^{MAX}) = \mathbf{j}^e \cdot \hat{\boldsymbol{n}}(\theta^{MAX}) = 0$ from which (2.31) follows. □

2.5 When, where and how much does crack propagate?

- When: when critical void fraction is reached, i.e., $\zeta = \zeta_{crit}$, cf. the model equations below (cf. Eq. (3.7)).
- Where: in the direction of θ^{MAX}, that is, as parallel to the tip traction cf. Eq. (2.18).
- How much: with a velocity V given by (2.25) while the quasistatic time-step δt is fixed.

3 Balance and flow laws

The solution will consis in solving coupled balance and flow lows.

3.1 Temperature-dependent compressible neo-Hookean isotropic finite strain elasticity

The (isotropic[6]) compressible neo-Hookean free energy reads [22]

$$W(\mathbf{F}, \mathbf{F^p}) := \frac{\mu}{2}\left(J_e^{-2/3}\,\mathrm{tr}\;\mathbf{b^e} - 3\right) + \frac{\kappa}{2}(1 - J_e)^2, \tag{3.1}$$

with $\mathbf{b^e} := \mathbf{F^e}\mathbf{F^e}^T$ and $J_e := \sqrt{\det\,\mathbf{b^e}}$. This energy is known to be well-defined for metal plasticity (where elastic strains are smaller than plastic strains). Note however that being non polyconvex, there exist no solution in the framework of pure nonlinear elasticity[7].

The associated temperature-dependent free energy reads

$$\hat{\Psi}(\mathbf{b^e}, T) := W(\mathbf{F}, \mathbf{F^p}) + (3\lambda + 2\mu)\tilde{\alpha}(T - T_{env})(1 - J_e) - \frac{C_p\rho}{2T_{env}}(T - T_{env})^2, \tag{3.2}$$

with $\tilde{\alpha}$ the coefficient of thermal expansion.

[6] As it depends on $\mathbf{b^e}$ only.

[7] In [20] the authors show that there is no existence of solutions for limit cases – cavitation, but however it should be noted that they consider a bulk energy density of the form $(\nabla\mathbf{u})^2$, which is far from being $\mathbf{F}\mathbf{F}^T$ and even less $\mathbf{F^e}\mathbf{F^e}^T$.

It follows that the Kirchhoff stress is defined as $\boldsymbol{\tau}(\mathbf{b^e}, T) := 2\dfrac{\partial \Psi}{\partial \mathbf{b^e}}\mathbf{b^e}$, that is, in plain stress (note that the factor $E/(1-\nu)$ sould be replaced by $(3\lambda + 2\mu)$ in plane strain or in $3D$) [7],

$$\boldsymbol{\tau}(\mathbf{b^e}, T) = \mu J_e^{-2/3}(\mathbf{b^e} - \frac{\text{tr } \mathbf{b^e}}{3}\mathbf{I}) - \left(\kappa(1-J_e) + \frac{\tilde{\alpha}E}{1-\nu}(T - T_{env})\right) J_e \mathbf{I}. \tag{3.3}$$

Remark that (2.14) is satisfied with τ as given by (3.3).

Assume that $\mathbf{b^e} \in L^2(\Omega)$ with $J_e \in L^\infty(\Omega)$. Since $\mathbf{b^e} = \mathbf{F C^{p}}^{-1}\mathbf{F}^T =: \hat{\mathbf{b^e}}(\mathbf{F(u)}, \mathbf{F^p}) = \tilde{\mathbf{b^e}}(\mathbf{u}, \mathbf{F^p})$ with $\mathbf{C^p} := \mathbf{F^p}^T\mathbf{F^p}$ and where $\mathbf{u}$ is the displacement field, the quasi-static momentum balance law in plane stress reads in the weak form: find $\mathbf{u} \in \left(H^1(\Omega)\right)^3$ such that:

$$\left\{ \begin{array}{rcl} \displaystyle\int_\Omega \boldsymbol{\tau}\left(\tilde{\mathbf{b^e}}(\mathbf{u}, \mathbf{F^p}), T\right) \cdot \nabla \hat{\mathbf{u}} dS & = & \displaystyle\int_{\Gamma^N} \mathbf{G} \cdot \hat{\mathbf{u}} dL \\ \tau_{33} & = & 0, \end{array} \right. \tag{3.4}$$

for every $\hat{\mathbf{u}} \in \left(H_0^1(\Omega; \mathbb{R}^3)\right)$ and where $\mathbf{G}$ is the applied load on the boundary (no external body forces are here considered).

The heat equation reads: find $T \in H^1(\Omega)$ such that:

$$\int_\Omega \left(\rho C_p \dot{T}\hat{T} + k\nabla T \cdot \nabla \hat{T}\right) dV = \int_\Omega \rho\bar{\alpha}\left(\boldsymbol{\tau} \cdot \mathbf{l^p}\right)\hat{T} dV, \tag{3.5}$$

for every $\hat{T} \in H_0^1(\Omega)$ and with $\bar{\alpha}$ the Taylor-Quinney coefficient (i.e., giving the proportion of energy converted into heat), and $\mathbf{l^p}$ the plastic strain rate to be defined below. The specific heat supply is given by

$$\dot{Q} = \bar{\alpha}\left(\boldsymbol{\tau} \cdot \mathbf{l^p}\right). \tag{3.6}$$

3.2 Principle of maximal plastic dissipation and flow law

Let us introduce the *maximal principal Almansi strain*

$$\epsilon_{eq} = \arg\max_{\epsilon_i}\Big\{ \det\ \Big((\mathbf{I} - \mathbf{b^e}^{-1}) - 2\epsilon_i \mathbf{I}\Big) = 0\Big\}, \tag{3.7}$$

the *void fraction* (that, is, the damage parameter),

$$\zeta = \left(\frac{\epsilon_{eq}}{\bar{\varepsilon}}\right)^2, \tag{3.8}$$

with $\bar{\varepsilon}$ a constitutive parameter. The m *yield functions* read $(1 \le i \le m = 2)$

$$\phi_i(\boldsymbol{\tau}, q_i; \zeta, T) \quad := \quad q_i - (1-\zeta)(1 - \frac{T - T_{env}}{T_{melt} - T_{env}})\sigma_y, \tag{3.9}$$

with T_{env} and T_{melt} the room and melting temperatures, respectively, with the *yield stress* given by

$$\sigma_y = \sigma_y^0 + \eta\bar{\epsilon}^p, \tag{3.10}$$

with σ_y^0 the initial tensile yield stress and η a material-hardening constitutive parameter, and where the von Mises and Drucker-Prager *equivalent stresses* read

$$\left\{ \begin{array}{rcl} q_1 = \sigma_1^{eq} & := & \sqrt{\frac{3}{2}\,\text{tr } \boldsymbol{\tau}^2 - \frac{1}{2}(\,\text{tr } \boldsymbol{\tau})^2} \\ q_2 = \sigma_2^{eq} & := & \sigma_1^{eq} - \beta\zeta\,\text{tr } \boldsymbol{\tau}. \end{array} \right. \tag{3.11}$$

with β a constitutive parameter.

Finally, by defining $\overset{\star}{\mathbf{b}}^{\mathbf{e}}$ as the derivative of $\mathbf{b}^{\mathbf{e}}$ while keeping $\mathbf{F}$ constant[8] (recall that $\mathbf{F} = \mathbf{F}^{\mathbf{e}}\mathbf{F}^{\mathbf{p}}$), we introduce the *plastic rate of deformation* as (cf. [7,16] for detail),

$$\mathbf{l}^{\mathbf{p}} := \dot{\mathbf{F}}^{\mathbf{p}}\mathbf{F}^{\mathbf{p}\,-1} = -\frac{1}{2}\,\overset{\star}{\mathbf{b}}^{\mathbf{e}}\,(\mathbf{b}^{\mathbf{e}})^{-1}, \tag{3.12}$$

whereby the *mechanical dissipation* reads (where Einstein summation applies),

$$\mathcal{D}\left(\boldsymbol{\tau}, q_i; \mathbf{l}^{\mathbf{p}}, \dot{\bar{\epsilon}}_i^p\right) := \boldsymbol{\tau}\cdot\mathbf{l}^{\mathbf{p}} - q_i\,\dot{\bar{\epsilon}}_i^p = \boldsymbol{\tau}\cdot(\mathbf{l}^{\mathbf{p}})^S - q_i\,\dot{\bar{\epsilon}}_i^p \tag{3.13}$$

with $\boldsymbol{\tau}\cdot\mathbf{l}^{\mathbf{p}}$ the rate of plastic dissipation, q_i the hardening stress corresponding to the ith yield function, and where the *equivalent plastic strain* $\bar{\epsilon}^p$ and *strain rate* $\dot{\bar{\epsilon}}^p$ defined as

$$\bar{\epsilon}^p := \sum_i \bar{\epsilon}_i^p = \sum_i \int_0^t \dot{\bar{\epsilon}}_i^p\, ds \quad \text{with} \quad \dot{\bar{\epsilon}}_i^p := \frac{\boldsymbol{\tau}\cdot\mathbf{l}^{\mathbf{p}}}{\sigma_i^{eq}}. \tag{3.14}$$

Theorem 2 (Maximal plastic dissipation) *The principle of maximal plastic dissipation entails the flow laws*[9]

$$\left\{\begin{array}{rcl} \frac{1}{2}\left(\mathbf{l}^{\mathbf{p}} + \mathbf{l}^{\mathbf{p}\,T}\right) & = & \displaystyle\sum_{i=1}^{2} \dot{\lambda}_i \frac{\partial \Phi_i}{\partial \boldsymbol{\tau}}(\boldsymbol{\tau}, q_i; \zeta, T) \\ \dot{\bar{\epsilon}}^p & = & \displaystyle -\sum_{i=1}^{2} \dot{\lambda}_i \frac{\partial \Phi_i}{\partial q_i}(\boldsymbol{\tau}, q_i; \zeta, T) \\ c\dot{\lambda}_i - \langle c\dot{\lambda}_i + \Phi_i(\boldsymbol{\tau}, q_i; \zeta, T)\rangle_+ & = & 0. \end{array}\right. \tag{3.15}$$

where the yield functions are given by (3.9).

Proof. In the set of admissible variables $(\boldsymbol{\tau}, q_i) \in \mathcal{A}$, the elasticity domain is defined as the subset $\Xi := \{(\mathbf{A}, a_i) \in \mathcal{A} \text{ s.t. } \phi^\star(\mathbf{A}, a_i; \zeta, T) \leq 0\}$ where $\mathbf{A}$ is a symmetric second-order matrix and a_i ($i = 1$ or 2), a scalar. Hill-Mandel's principle of maximal dissipation states that the solution $(\boldsymbol{\tau}, q)$ satisifies

$$\mathcal{D}\left(\boldsymbol{\tau}, q_i; \mathbf{l}^{\mathbf{p}}, \dot{\bar{\epsilon}}^p\right) = \max_{(\mathbf{A}, a_i)\in\Xi} \left\{\mathcal{D}\left(\mathbf{A}, a_i; \mathbf{l}^{\mathbf{p}}, \dot{\bar{\epsilon}}^p\right)\right\}. \tag{3.16}$$

Let us introduce the total yield function as $\Phi^\star = \Phi_1$ if $\phi_1 \leq 0$ and $\Phi^\star = \Phi_2$ if $\phi_1 > 0$. Remark that the condition $\Phi^\star\dot{\gamma} = 0$ can be rewritten as $\Phi^\star\dot{\gamma} = \displaystyle\sum_{i=1}^{2} \dot{\gamma}_i\phi_i = 0$ where $\dot{\gamma}_1(\tau) = 0$ if $\phi_1 > 0$ and $\dot{\gamma}_2(\tau) = 0$ if $\phi_1 \leq 0$.

From the constraint $\Phi^\star \leq 0$, the flow rules immediately follow from the stationary points of the Lagrangean $\mathcal{L}(\mathbf{A}, a_i, \dot{\lambda}; \mathbf{l}^{\mathbf{p}}, \dot{\bar{\epsilon}}^p) := -\mathcal{D}(\mathbf{A}, a_i; \mathbf{l}^{\mathbf{p}}, \dot{\bar{\epsilon}}^p) + \dot{\lambda}\Phi^\star(\mathbf{A}, a_i; f, T)$ w.r.t $(\mathbf{A}, a_i, \dot{\lambda})$ with the Lagrange multiplier $\dot{\lambda}$ and recalling definition (3.13). □

Let us remark that Eq. (3.15c) is solved directly by means of Chen-Mangasarian function [19]. Moreover $\dfrac{\partial\Phi^\star}{\partial\boldsymbol{\tau}}$ is computed in an exact manner with Mathematica [41].

For a detailed description of the numerical implementation of the model, of computational issues such as mesh opening, remeshing, type of finite elements used we refer to [7–9, 11]. Some detail is given in Section 4.2.

---

[8] As $\overset{\star}{\mathbf{b}}^{\mathbf{e}}$ represents the variation of $\mathbf{b}^{\mathbf{e}}$ due to permanent deformations while the total deformation is kept unchanged, it vanishes in the case of pure elastic unloading.

[9] Noting in passing that the extremization principles has left $\frac{1}{2}\left(\mathbf{l}^{\mathbf{p}} - \mathbf{l}^{\mathbf{p}\,T}\right)$ undefined, a fact that is not mentioned clear in classical literature. Let us also remark that the set of inequalities for the plastic multiplier and the yield function is given by the formal Eq. (3.15)c where c is a parameter to satisfy unit constitency.

4 Numerical implementation

4.1 Brief discussion on the numerical method

Combination of the return-mapping technique [39, 45] and mixed formulations [18] led to a standardization of elasto-plastic modeling with finite elements (see the treatise by Belytschko et al. [15] and the one by Bonet [16]). However, return-mapping algorithms where implicit inequality for the plastic multiplier appear still pose challenges to systematization, since the predictor in the presence of ductile damage evolution can give a false indication and might produce fictitious unloading. As a consequence, classical finite strain constitutive approaches (e.g. the rotated $\mathbf{F^e F^p}$ method [5]) inherit some of the difficulties of the small strain algorithms.

Besides these problems, in complex simulations the convergence radius is often not satisfactory [21]. For ductile fracture problems, where mesh adaptation, quadrature point alterations and even full remeshing has to be adopted, small convergence radius can be impairing for a successful analysis.

Here, the finite strain elasto-plastic algorithm of [7] has been adopted, which allows us to include in the same underlying framework, kinematic hardening, anisotropy and damage. Adding to this, recent ductile damage models (specifically the one by Areias et al. [10]) make use of non-differentiable convex yield functions, not easily tractable by classical return-mapping algorithms.

4.2 Iteration of the historical variables

The time interval $[0, t^\star]$ is discretized and the unknown are computed at time $t^n \in [0, t^\star]$ with $1 \leq n \leq N$.

To find $\mathbf{F}$ and T at each time iteration, we need to determine the tangent modulus associated to (3.4) and (3.5),

$$\begin{bmatrix} \frac{\partial \dot{Q}}{\partial T} & \frac{\partial \dot{Q}}{\partial \mathbf{F}} \\ \frac{\partial \boldsymbol{\tau}}{\partial T} & \frac{\partial \boldsymbol{\tau}}{\partial \mathbf{F}} \end{bmatrix},$$

which is computed with Mathematica and the *AceGen* add-on [30].

Then, having solved (3.4) at time t_{n+1} knowing the solution at time t_n, the increment of $\mathbf{F}$ is found as

$$\delta \mathbf{F_n} = \mathbf{F_{n+1}} {\mathbf{F_n}}^{-1}.b$$

From the expression $\mathbf{b^e} = \mathbf{F} {\mathbf{C^p}}^{-1} \mathbf{F}^T$ we infer that $\mathbf{b^e}$ at time t_{n+1} writes as

$$\mathbf{b^e_{n+1}} = \mathbf{F_{n+1}} {\mathbf{C^p}_n}^{-1} {\mathbf{F_{n+1}}}^T + \delta \overset{\star}{\mathbf{b}}{}^{\mathbf{e}}_{\mathbf{n}} = \mathbf{F_{n+1}} \left({\mathbf{F_n}}^{-1} \mathbf{b^e_n} {\mathbf{F_n}}^{-T} \right) {\mathbf{F_{n+1}}}^T + \delta \overset{\star}{\mathbf{b}}{}^{\mathbf{e}}_{\mathbf{n}} = \delta \mathbf{F_n} \mathbf{b^e_n} \delta {\mathbf{F_n}}^T + \delta \overset{\star}{\mathbf{b}}{}^{\mathbf{e}}_{\mathbf{n}}$$

where $\delta^\star \mathbf{b^e}$ is the increment of $\mathbf{b^e}$ caused by a variation of $\mathbf{C^p}$. In brief we write

$$\mathbf{b^e_{n+1}} = \mathbf{b^{e^\circ}_n} + \delta \overset{\star}{\mathbf{b}}{}^{\mathbf{e}}_{\mathbf{n}} \tag{4.1}$$

where $\mathbf{b^{e^\circ}_n}$ is the "trial" $\mathbf{b^e}$ at time t^n. Then $\boldsymbol{\tau_n} := \boldsymbol{\tau}(\mathbf{b^e_n}, T_n)$ is replaced by $\boldsymbol{\tau_{n+1}}$ and (3.4) is solved iteratively as coupled with the heat equation.

On the other hand $\mathbf{d^p} := (\mathbf{l^p})^S = -\frac{1}{4} \overset{\star}{\mathbf{b}}{}^{\mathbf{e}} (\mathbf{b^e})^{-1} - \frac{1}{4} (\mathbf{b^e})^{-1} \overset{\star}{\mathbf{b}}{}^{\mathbf{e}}$ which as rewritten in Voigd form allows us to isolate $\overset{\star}{\mathbf{b}}{}^{\mathbf{e}}$, that is,

$$\mathbf{d^p_V} = -\frac{1}{4} \boldsymbol{A_V} \overset{\star}{\mathbf{b}}{}^{\mathbf{e}}_{\mathbf{V}} \tag{4.2}$$

where in $3D$, $\boldsymbol{A_V}$ is a 6×6 matrix whose entries are linear combinations of the entries of $(\mathbf{b^e})^{-1}$ [7].

As a consequence, the flow law (3.15) is integrated semi-implicitly. In particular, matrix A is kept constant as a function of $\mathbf{b^e_n}$ and then the flow law reads as the nonlinear system (Voigt notation is used):

$$\left\{ \begin{array}{rcl} 0 & = & \mathbf{b^{e^\circ}_n} - \mathbf{b^e_{n+1}} - 4 \boldsymbol{A}^{-1}_{\boldsymbol{V}\boldsymbol{n}} \boldsymbol{n}_n \cdot \delta \dot{\gamma} \\ 0 & = & \bar{\epsilon}^p_n - \bar{\epsilon}^p_{n+1} + \varphi_n \delta \dot{\gamma} \\ 0 & = & c \delta \dot{\gamma} - \langle \mathbf{c} \delta \dot{\gamma} + \delta \varphi \rangle_+ \end{array} \right. , \tag{4.3}$$

with the flow vector $\boldsymbol{n}_n := \left(\frac{\partial \Phi_1}{\partial \boldsymbol{\tau}}, \frac{\partial \Phi_2}{\partial \boldsymbol{\tau}}\right)(\boldsymbol{\tau_{n+1}}, q_{i_{n+1}}; \zeta_n, T_{n+1})$ and $\varphi_n := \left(\frac{\partial \Phi_1}{\partial q_1}, \frac{\partial \Phi_2}{\partial q_2}\right)(\boldsymbol{\tau_{n+1}}, q_{i_{n+1}}; \zeta_n, T_{n+1})$. Moreover, the notation $\delta\dot{\gamma} = (\delta\gamma_{\mathbf{1}}, \delta\gamma_{\mathbf{2}})^{\mathbf{T}}$, $\delta\boldsymbol{\Phi} = \left(\delta\boldsymbol{\Phi_1}, \delta\dot{\boldsymbol{\Phi}}_{\mathbf{2}}\right)^{\mathbf{T}}$, $\delta\varphi = (\delta\varphi_{\mathbf{1}}, \delta\varphi_{\mathbf{2}})^{\mathbf{T}}$ is employed.

The solution of (4.3) provides the constitutive variables at time t^{n+1},

$$\{\mathbf{b^e_{n+1}}, \delta\dot{\gamma}, \bar{\epsilon}^{\mathbf{p}}_{\mathbf{n+1}}\}^{\mathbf{T}}.$$

A figure summarizing the iterative process is provided in Fig. 3. Supplementary detail on the numerical resolution of (4.3) can be found in [7, 9].

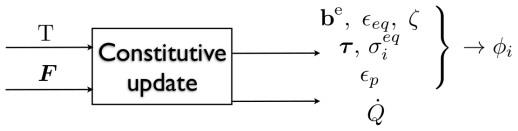

Figure 3: Summary of the iterative process.

4.3 Smoothing the complementarity condition

Equation (4.3*c*) is solved be approximating the "plus" function $\langle\cdot\rangle_+$ by the smooth ramp function [19],

$$\langle x\rangle_+ \sim S(x) \quad = \quad x + \frac{1}{\alpha_e}\ln\left(1 + \exp(-\alpha_e x)\right),$$

as can be observed in Fig. 4.

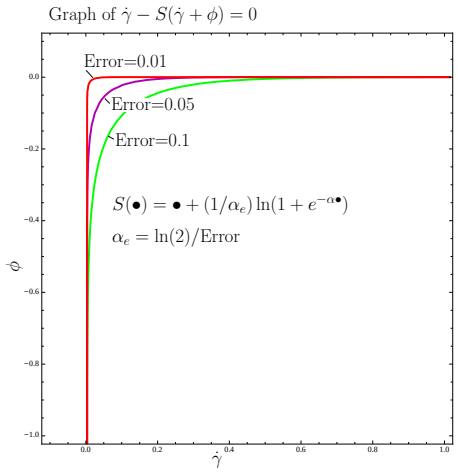

Figure 4: Approximation of the "plus" function to solve the complementarity conditions (i.e., the flow rules).

4.4 Computation of the contour integral and fracture algorithm

The crack tip traction $\mathbf{j}^{\mathbf{e}}$ whose expression is given by (2.18) is computed in the reference configuration as a contour integral on a circle centered at the crack tip and of radius 1/40th of the body diameter.

A picture of the fracture algorithm is provided in Fig. 5.

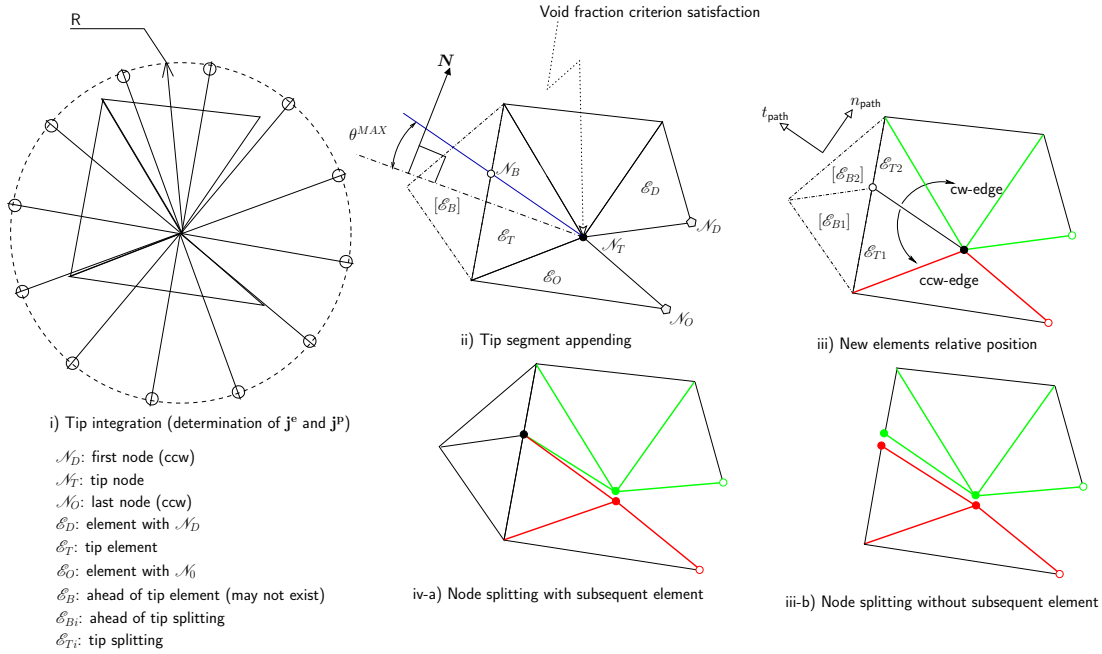

Figure 5: Fracture algorithm. Left: the contour integral: the stress is interpolated at 100 points on the circle of radius R; Middle: node splitting and mesh opening; Right: element re-ordering and splitting.

5 Numerical results

Concerning the algorithm, direct integration of the rate equations is performed as well as smoothing of the complementarity conditions with the Chen- Mangasarian function. The resulting problem is smooth, always converges quadratically and is robust, typically requiring fewer steps than return-mapping algorithms.

Selected examples are shown in the following sections. In the first 2 and last examples no thickness variation was considered. The second example is then re-run with thickness variation (see §5.3) showing no significant change in the results.

5.1 Ductile fracture in Mode 1 and Mode 2

The fracture model as based on configurational forces is first tested on classical Mode I and Mode II loading experiments. The set-up and the values of the model parameter are shown in Fig. 6. The mode I loading (i.e., pure traction) consists in a imposed displacement perpendicular to the upper and lower faces of the body, while the left-side face is clamped and right-side face is displacement free. For the mode II loading (i.e., pure shear) the imposed displacement is parallel to the upper and lower faces. The left-side face is clamped in its upper half part and force-free in its lower half part, while the right-side face is also force-free. In both cases a notch is inserted in the middle of the left-side face.

Propagation of the crack as loading increases is observed in Figs. 7 (for mode I) and 9 (for mode II) along a path whose direction is given by the principle of maximal dissipation and hence with a kinking angle given by the direction of the tip traction (2.18). The time increment is here 0.1 s. The temperature dependent elasto-plastic problem is solved entirely at each iteration: effective plastic strain, damage and temperature difference (i.e., $T - T_{env}$) are shown in Figs. 7 and 9, while load-displacement curves are given in Figs. 8 (for mode I) and 10 (for mode II) for 2 mesh refinements, which are shown in Fig. 11.

It is astonishing to observe that the path followed by the Mode I and Mode II cracks are almost identical. In fact, one knows that in brittle fracture the two paths are clearly distinct (cf., e.g., [1]). However, for ductile fracture this is no more the case as laboratory experiments and numerical

simulations show [2, 27, 36, 47].

From this consideration, it appears mandatory to assess our model with comparison with these known experimental facts. This is done in §5.2

$E = 210$ GPa
$\nu = 0.3$
$\sigma_y = 500 + 1500\overline{\varepsilon}_p$ Mpa
$\beta = 3$
$\overline{\varepsilon} = 0.8$
$T_{\text{env.}} = 20$ °C
$T_{\text{melt}} = 1535$ °C
$m = 2$
$\widetilde{\alpha} = 1.2 \times 10^{-5}$ K^{-1}

$\overline{\alpha} = 0.9$
$\rho = 7850$ Kg/m^3
$k = 60$ W/(m· K)
$C_p = 460$ J/(Kg· K)
$\zeta_{\text{crit}} = 0.05$

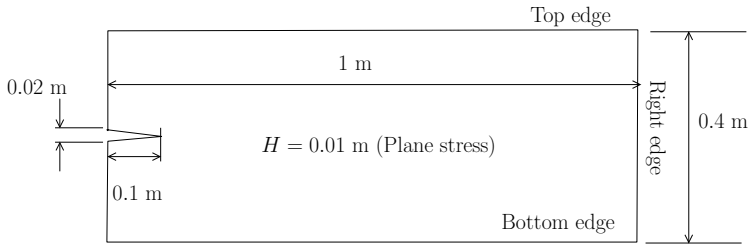

Coarse mesh: 3267 nodes, 6284 elements
Fine mesh: 12870 nodes, 25240 elements
Top edge: $v_y = 1$ ms^{-1} (mode I), $v_x = 5$ ms^{-1} (mode II)
Bottom edge: $v_y = -1$ ms^{-1} (mode I), $v_x = -5$ ms^{-1} (mode II)
Right edge: $v_x = 0$ (mode I)

Figure 6: The set-up and all values of the material and model parameter for the Mode I and Mode II experiments.

5.2 The Arcan-Sutton tearing test

The Arcan test fixture as shown in Fig. 13 have been originally used for testing of composite specimens for stable tearing tests [3]. We here refer to Sutton et al. [47] where experimental results by Amstutz et al. [2] have been reproduced with good qualitative agreement for 2024-T3 aluminum.

Our objective is to assess our criterion based on maximal dissipation and our temperature-dependent finite-strain elasto-plastic model by comparison of the numerically computed crack propagation direction with the known experimental paths for a series of 5 mixed-mode loading angle.

The results shown in Fig. 14 indicate good agreement with the experimental results. The time increment is here 0.1 s. The temperature is also shown along the path in Fig. 14. Therefore it is believed that the proposed model deserves attention towards future applications of ductile fracture.

5.3 ARCAN test with plane stress and thickness variation

Thickness variation is caused by the condition $\tau_{33} = 0$ where 3 is the out-of-plane direction. Since the deformation gradient for plane stress can be partitioned as

$$\mathbf{F} = \begin{bmatrix} F_{11} & F_{12} & 0 \\ F_{22} & F_{21} & 0 \\ 0 & 0 & F_{33} \end{bmatrix} \tag{5.1}$$

where

$$F_{33} = \frac{h}{H} \tag{5.2}$$

with h and H representing, respectively, the deformed and undeformed thickness, we can therefore

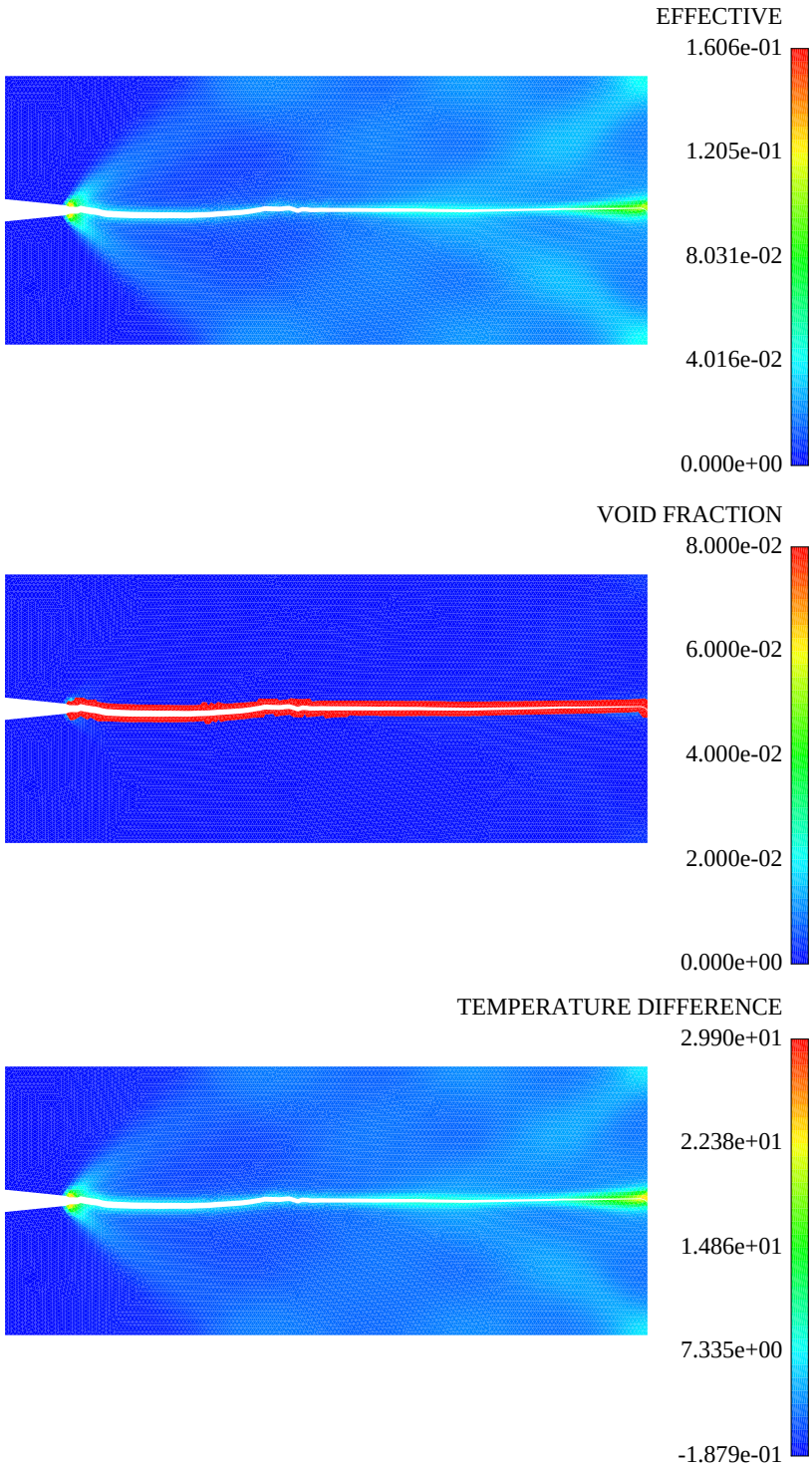

Figure 7: The effective plastic strain, the damage (i.e., void fraction) parameter and the temperature for the Mode I experiment. The time increment is here 0.1 s.

impose the condition $\tau_{33} = 0$ by calculating F_{33} and therefore h. The application of Newton's method results as:

$$\frac{\partial \tau_{33}}{\partial F_{33}} \delta F_{33} = -\tau_{33} \tag{5.3}$$

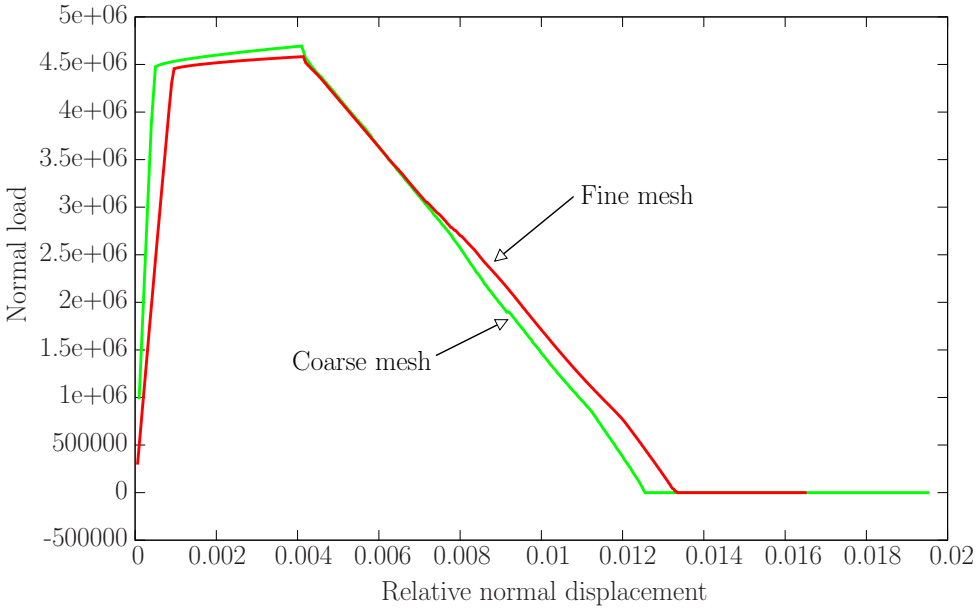

Figure 8: Displacement-loading curves for coarse and fine meshes for the Mode I experiment. A first stable process is followed by an unstable propagation. Coarse mesh consists of 3270 nodes and 6284 elements. Fine mesh consists of 12870 nodes and 25240 elements.

Further details concerning this topic can be consulted in Areias et al. [11]. Simulation results of thickness variation are shown in Fig. 15. Corresponding velocity profiles at the crack tip are shown in Fig. 16

5.4 Force-free elasto-plastic fracture

Crack opening by pure cooling can also be simulated with our method. Heat is flowing throughout the horizontal faces, while no forces are exerted on the boundary. The time increment is here 1.5 s. The crack path is determined by the tip traction by means od (2.18), where the dependence of $\mathbf{P}$ on the temperature is explicitely provided by the formula $\mathbf{P} = \boldsymbol{\tau}\mathbf{F}^{-T}$ with $\boldsymbol{\tau} = \hat{\boldsymbol{\tau}}(\mathbf{b}^{\mathbf{e}}, T)$ given by (3.3). All other field dependence on the temperature are implicitely provided by the flow law, the momentum and the heat equations. Set-up and results are shown in Fig. 18.

Moreover, load-displacement curves are also provided in Fig. 18 for 2 mesh refinements, which are the same as those of Fig. 11.

6 Concluding remarks

The first aim of this paper was to providing a complete fracture simulation model for finite-strain metal plasticity with as few as possible *model parameters*. In total there are 7 parameters, 5 of which are specifically designed for the plastic model, while 2 only are specific for the fracture model. There are 2 parameters in the yield stress expression (3.10), 1 for the damage parameter (3.7), and 1 in the Drucker-Prager equivalent stress (3.11a), while the last plastic parameter is m, the chosen number of plastic surfaces. Concerning crack propagation one needs to provide ζ_{crit}, the chosen threshold for complete softening (at which crack begins to propagate) and R the radius of the contour to compute the crack tip traction in (2.18). In the above simulations the value of R was 1/40th of the body diameter.

The second objective was to be able to justify the model in a deductive manner and this was

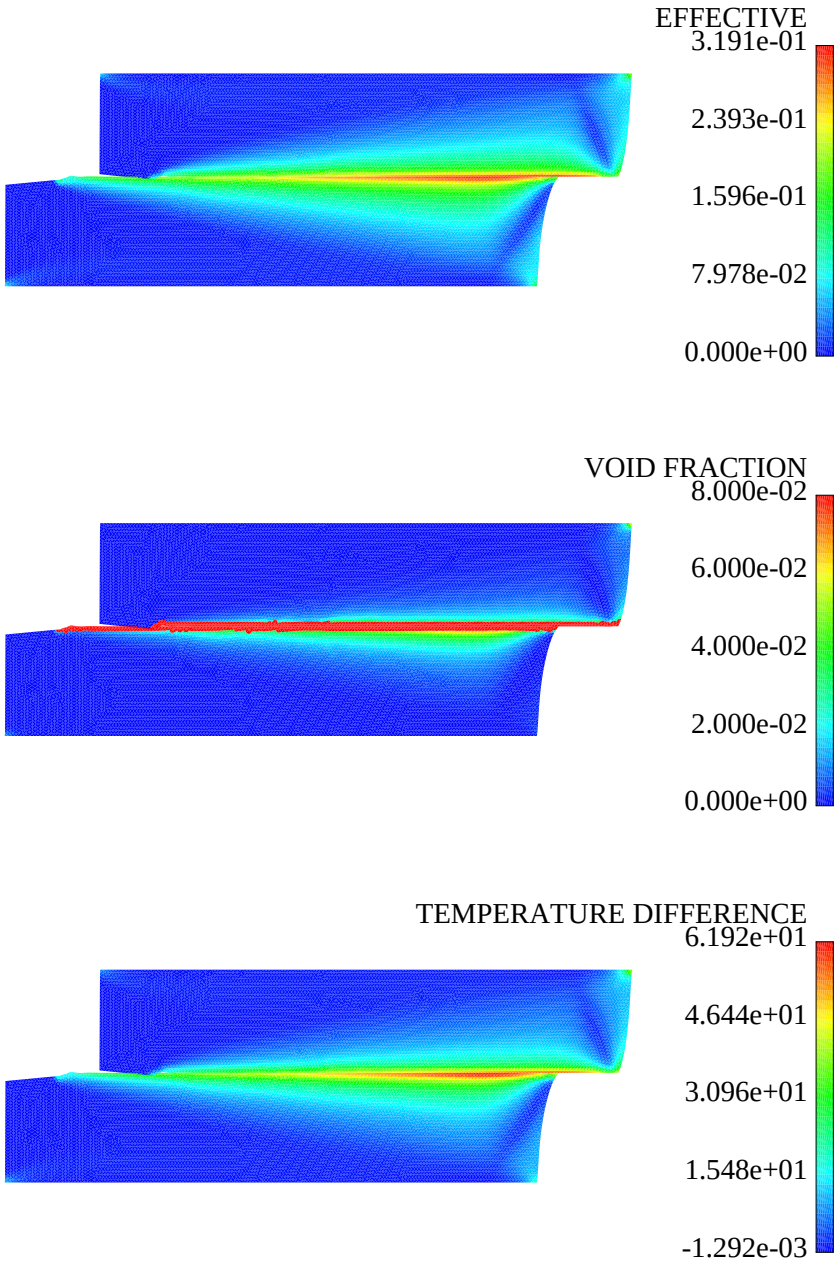

Figure 9: The effective plastic strain, the damage (i.e., void fraction) parameter and the temperature for the Mode II experiment. The time increment is here 0.1 s.

possible by appealing to Gurtin's notion of *configurational force* [26]. The main interest is then to understand fracture mechanisms, since they follow from rational arguments which can be validaded and analyzed by comparing numerical simulation as based on the model with experimental data. This was done in Section 5.

Let us also remark that the theory provides an explicit expression of the crack tip speed, which we have features for one simulation example in Fig. 16. To the knowledge of the authors, such an explicit crack tip speed expression in the quasi-static setting is not found in the literature on computrational fracture. Let us emphasize that our expression (2.25) comes directly from Gurtin's work [26], which has served as foundation of our method, model and algorithm.

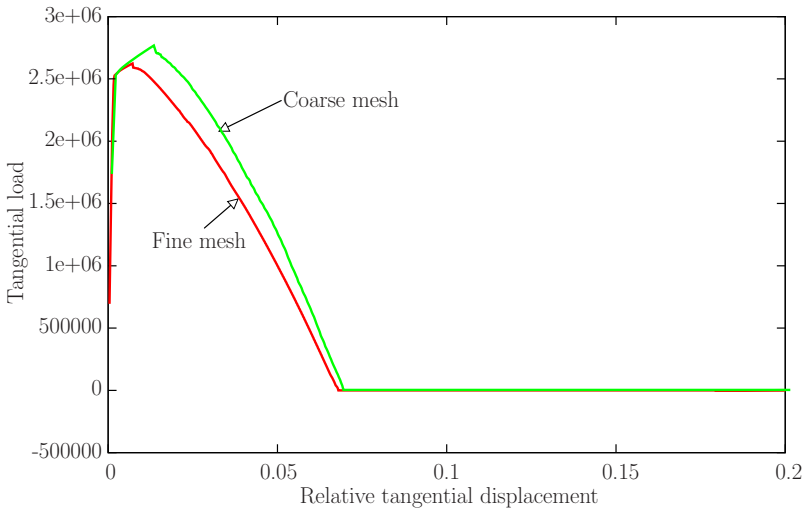

Figure 10: Displacement-loading curves for coarse and fine meshes for the Mode II experiment. A first stable process is followed by an unstable propagation.

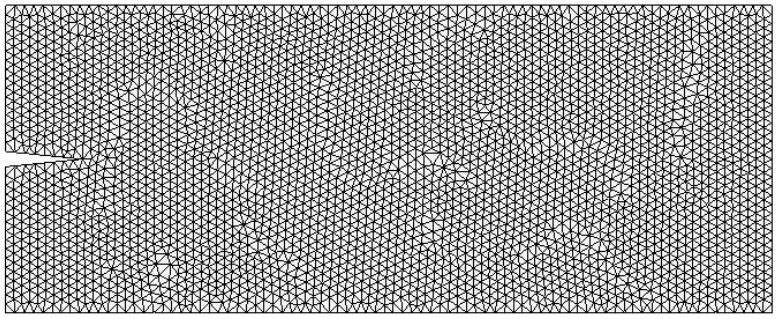

(a)

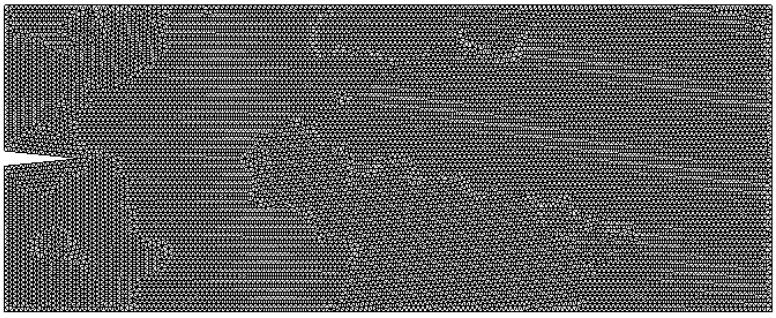

(b)

Figure 11: 11(a) Coarse mesh consisting of 3270 nodes and 6284 elements. 11(b) Fine mesh consisting of 12870 nodes and 25240 elements.

The third goal was to develop a numerical scheme to solve the global problem which is both *nonlinear and non smooth*, cf. Section 3. These algorithmic and computational aspects have been less explained in the present paper, since it is based on the SIMPLAS code [4] whose various ingredients and features have been previously published [6–8, 11].

The present paper then focusses on the two novel aspects of the model, namely the temperature

$E = 73.1$ GPa
$\nu = 0.33$
$\sigma_y = 344 + 769.44\bar{\varepsilon}_p$ Mpa for $\bar{\varepsilon}_p \leq 0.18$
$\sigma_y = 483 + 45.122(\bar{\varepsilon}_p - 0.18)$ Mpa for $\bar{\varepsilon}_p > 0.18$
$\beta = 3$
$\overline{\varepsilon} = 0.18$
$T_{\text{env.}} = 20$ °C
$T_{\text{melt}} = 502$ °C
$m = 2$
$\widetilde{\alpha} = 2.3 \times 10^{-5}$ K^{-1}

$\overline{\alpha} = 0.9$
$\rho = 2780$ Kg/m^3
$k = 121$ W/(m· K)
$C_p = 875$ J/(Kg· K)
$\zeta_{\text{crit}} = 0.2$

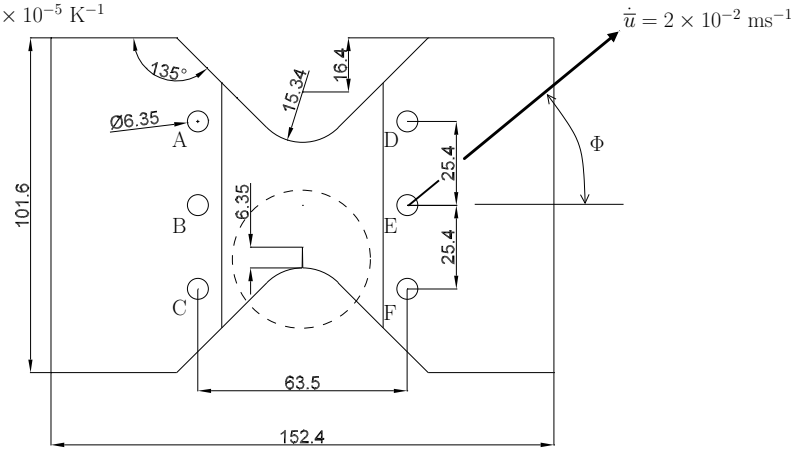

All dimensions in mm

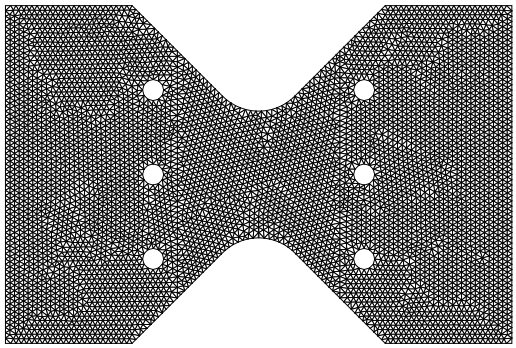

Mesh: 5721 nodes, 11017 elements

Figure 12: The Arcan set-up (top) and mesh (bottom) and all values of the material and model parameter as based on [3, 47].

dependence and the crack propagation criterion as based on configurational forces. This latter point is crucial since we believe that its major advantage is its *generality*: a mere modification of the free energy is automatically taken into account in the fracture criterion. For instance if a dislocation model or an electro-magnetic coupling is added to the current thermodynamic model, the specific role played by the dislocations or the Lorentz force on the crack path direction might be accounted for without requiring further ad-hoc procedures. Moreover, as opposed to many other methods based on this notion, here the contour integral is solved directly without need to finely mesh the tip region, which is computationally expensive (and requires to compute the higher order terms).

The specific role of the temperature on crack propagation has also been investigated. Our first concern was to include thermal effects, since temperature is a thermodynamic variable of major importance in every physical mechanism where dissipation plays a crucial role. This is why the temperature appears explicitly or implicitly in every model equation, including of course in the tip traction expression which determines the kinking direction. Moreover, temperature dependence has

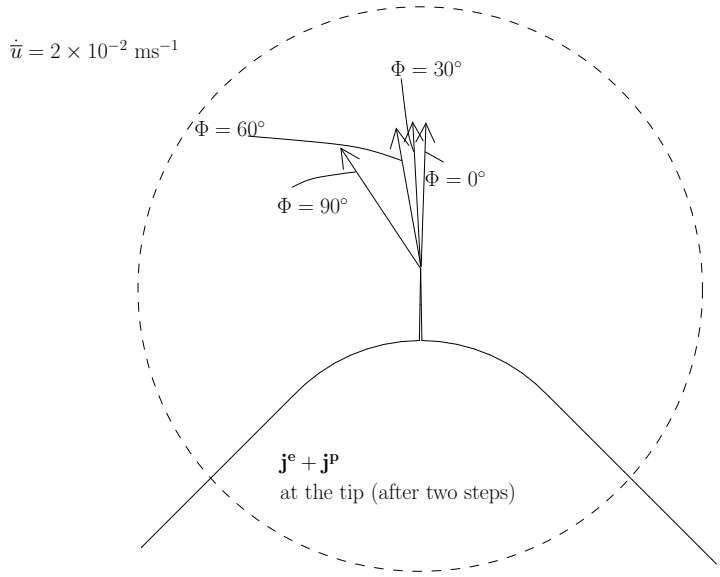

Figure 13: Configurational forces after 2 time steps in the Arcan test.

been incorporated also because thermal gradients do play a role in the physical mechanisms of fracture. As a matter of fact, our last numerical simulation shows that force-free fracture can also be predicted.

Since the Arcan-Sutton experimental curves have been reproduced with our method (cf. §5.2) with reasonable accuracy, we believe that our results constitute a solid basis to further analyze fracture, by developing and applying the method to other physical effects. This will be done in future work.

References

[1] G. Allaire, F. Jouve, and N. Van Goethem. Damage and fracture evolution in brittle materials by shape optimization methods. *J. Comput. Physics*, 33(16):5010–5044, 2011.

[2] B.E. Amstutz, M.A. Sutton, D.S. Dawicke, and J.C. Newman Jr. An experimental study of ctod for mode I/II stable crack growth in thin 2024-t3 aluminum specimens. *Fracture Mechanics ASTM*, STP 125:256–271, 1995.

[3] M. Arcan, Z. Hashin, and A. Voloshin. A methods to produce uniform plane stress state with applications to fiber-reinforced materials. *Experimental Mechanics*, 18:141–146, 1978.

[4] P. Areias. Simplas. https://ssm7.ae.uiuc.edu:80/simplas.

[5] P. Areias and T. Belytschko. Analysis of finite strain anisotropic elastoplastic fracture in thin plates and shells. *J Aerospace Eng*, 19(4):259–270, 2006.

[6] P. Areias, D. Dias-da-Costa, J. Alfaiate, and E. Júlio. Arbitrary bi-dimensional finite strain cohesive crack propagation. *Comput Mech*, 45(1):61–75, 2009.

[7] P. Areias, D. Dias da Costa, J., E.B. Pires, and J. Infante Barbosa. A new semi-implicit formulation for multiple-surface flow rules in multiplicative plasticity. *Comput Mech*, 49:545–564, 2012.

[8] P. Areias and T. Rabczuk. Smooth finite strain plasticity with nonlocal pressure support. *Int J Numer Meth Eng*, 81:106–134, 2010.

[9] P. Areias, T. Rabczuk, D. Dias da Costas, and E.B. Pires. Implicit solutions with consistent additive and multiplicative components. *Finite Elements in Analysis and Design*, 57:15–31, 2012.

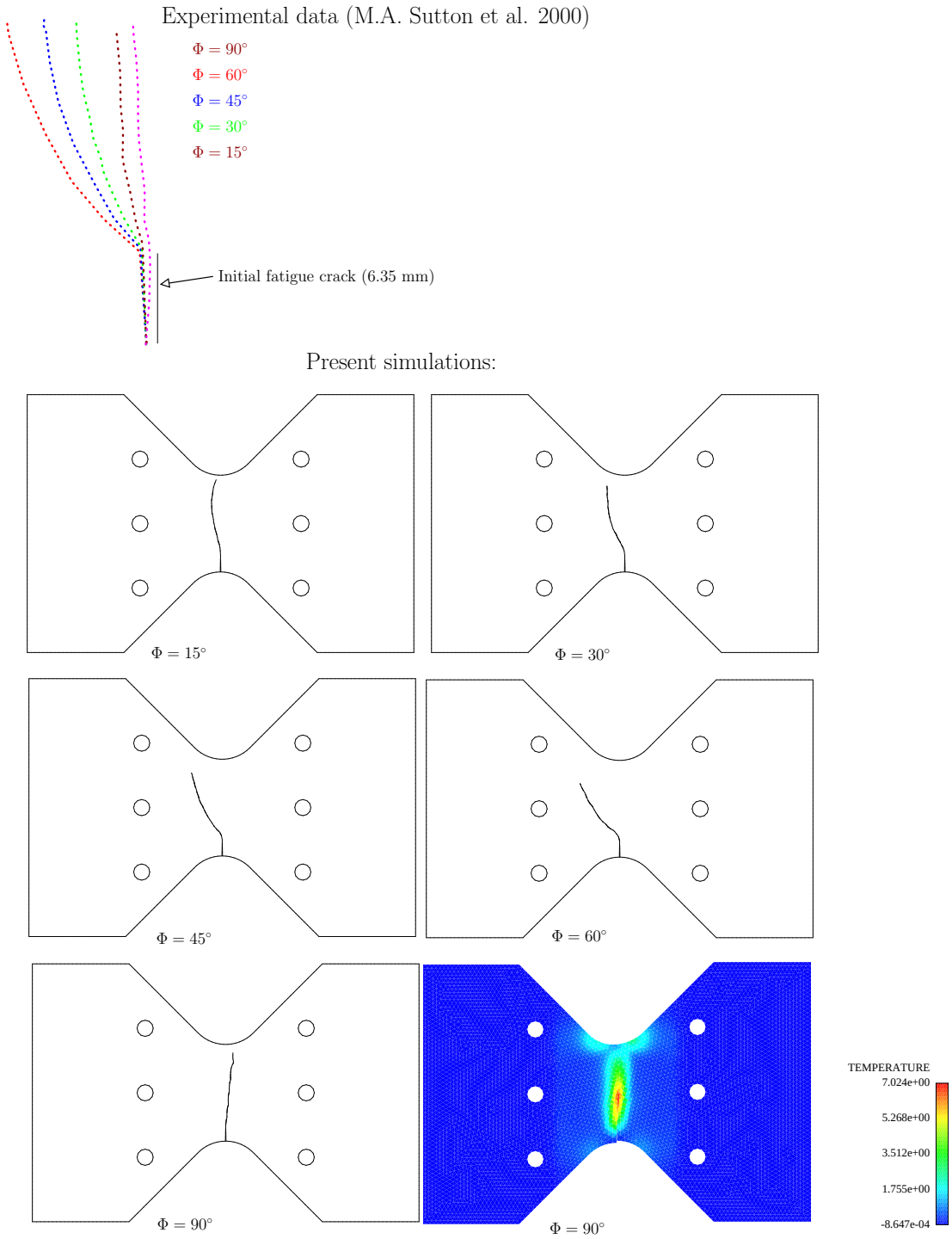

Figure 14: The crack paths provided by our model as based on configurational forces. The time increment is here 0.1 s.

[10] P. Areias, N. Van Goethem, and E.B. Pires. Constrained ale-based discrete fracture in shells with quasi-brittle and ductile materials. In *CFRAC 2011 International Conference*, Barcelona, Spain, June 2011. CIMNE.

[11] P. Areias, N. Van Goethem, and E.B. Pires. A damage model for ductile crack initiation and propagation. *Comput Mech*, 47(6):641–656, 2011.

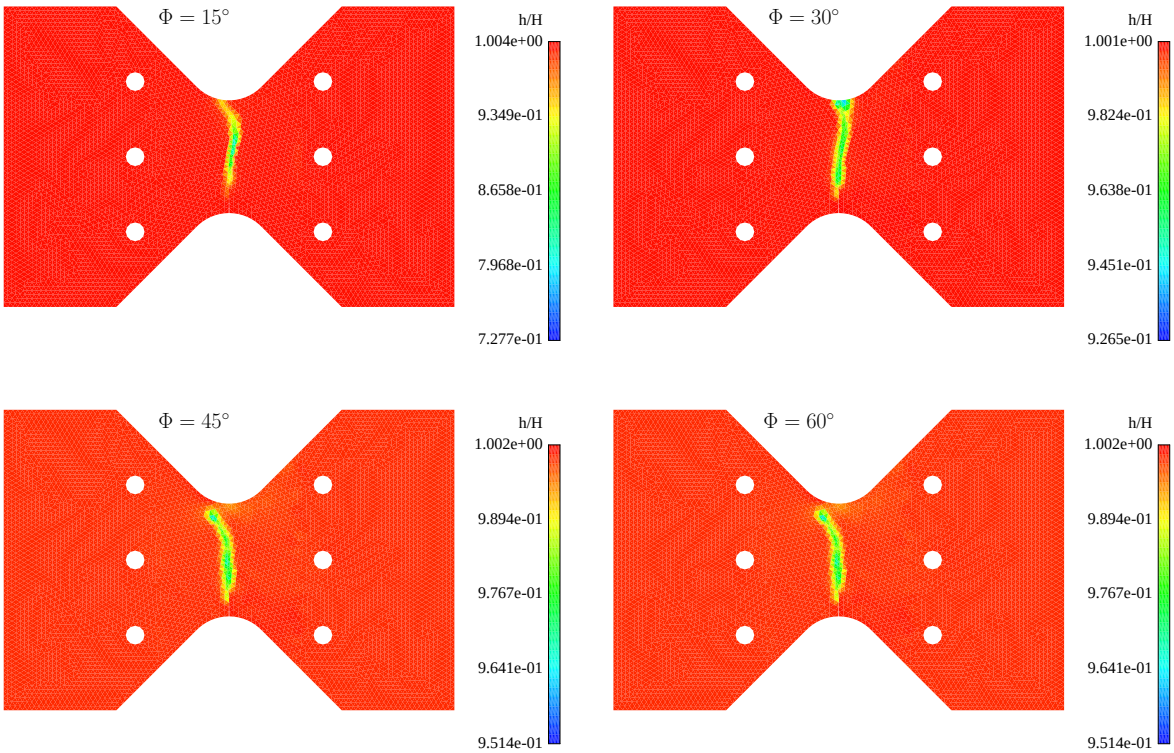

Figure 15: Thickness variation in the Arcan-Sutton test performed (coarse mesh)

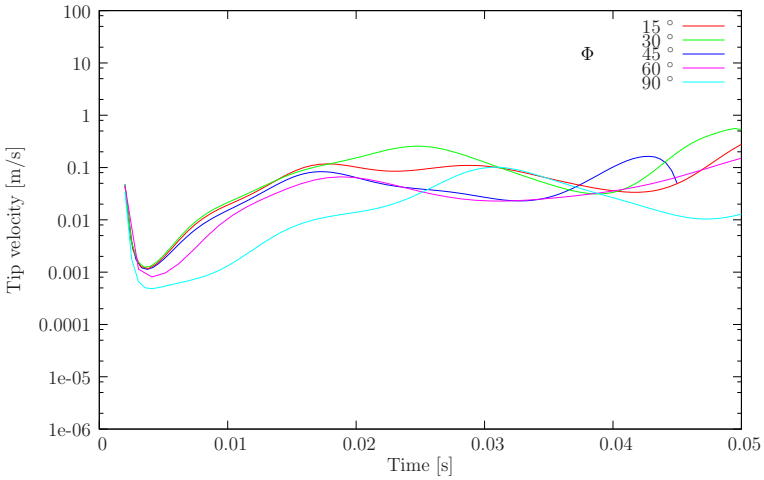

Figure 16: Crack tip speed as given by Eq. (2.25) in the Arcan-Sutton test with thickness variation (coarse mesh)

[12] C. J. Larsen B. Bourdin and C. L. Richardson. A time-discrete model for dynamic fracture based on crack regularization. *International Journal of Fracture*, 168(2):133–143, 2011.

[13] G.I. Barenblatt. On the equilibrium cracks due to brittle fracture. *Doklady AN SSSR*, 127:47–50, 1959. (In Russian).

[14] Z.P. Bažant. Instability, ductility and size effect in strain softening concrete. *J Eng Mech Div-ASCE*, 102:331–344, 1976.

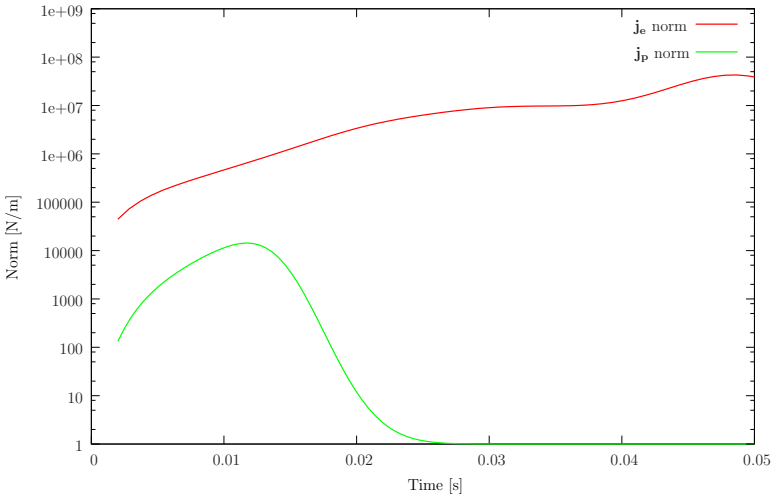

Figure 17: Comparison between $\mathbf{j^e}$ and $\mathbf{j^p}$ to validade Assumption 3 (coarse mesh and $\Phi = 15°$): it is observed that $\|\mathbf{j^e}/\|\mathbf{j^p}\|$ is of the order of 0.1%.

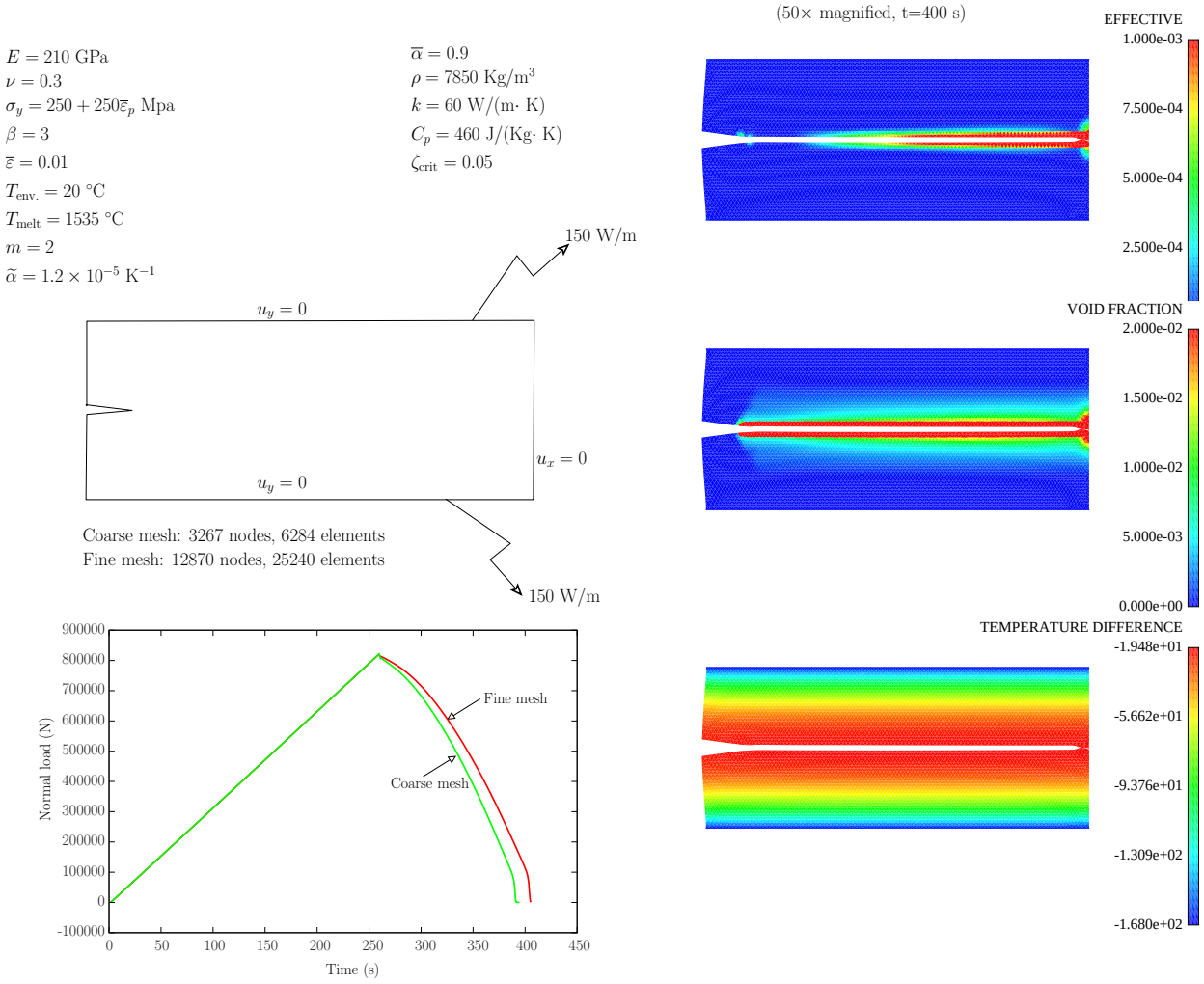

Figure 18: Crack opening by pure cooling with our model as based on configurational forces.

[15] T. Belytschko, W.K. Liu, and B. Moran. *Nonlinear finite elements for continua and structures*. John Wiley & Sons, 2000.

[16] J. Bonet and R.D. Wood. *Nonlinear Continuum Mechanics for Finite Element Analysis*. Cambridge University Press, Second edition, 2008.

[17] B. Bourdin, G. Francfort, and J.J. Marigo. *The Variational Approach to Fracture*. Springer-Verlag, 2008.

[18] F. Brezzi and M. Fortin. *Mixed and hybrid finite element methods*. Springer, 1991.

[19] C. Chen and O.L. Mangasarian. A class of smoothing functions for nonlinear and mixed complementarity problems. *Comput Optim Appl*, 5:97–138, 1996.

[20] S. Conti and C. de Lellis. Remarks on the theory of elasticity. *Annali della Scuola Normale Superiore di Pisa - Classe di Scienze, Ser. 5*, 2(3):521–549, 2003.

[21] M.A. Crisfield and V. Norris. A stabilized large-strain elasto-plastic $Q_1 - P_0$ method. *Int J Numer Meth Eng*, 46:579–592, 1999.

[22] I. Doghri. *Mechanics of Deformable Solids: Linear, Nonlinear, Analytical and Computational Aspects*. Springer, 2000.

[23] A. Gupta and X. Markenscoff. An anisotropic elastic formulation for configurational forces in stress space. *Int. J. Fract.*, 147(1-4):157–161, 2007.

[24] A. Gupta and X. Markenscoff. Configurational forces as dissipative mechanisms: a revisit. *C. R., Méc., Acad. Sci. Paris*, 336(1-2):126–131, 2008.

[25] M.E. Gurtin. *Topics in Finite Elasticity*. SIAM, 1981.

[26] M.E. Gurtin. *Configurational Forces as Basic Concepts of Continuum Physics*. Applied Mathematical Sciences, 137. Springer, 2000.

[27] M.A. James and D. Swenson. *A software framework for two-dimensional mixed mode I/II elastic-plastic fracture*. K. J. Miller and D. L. McDowell(Ed.), Mixed Mode Crack Behavior ASTM STP 1359. ASTM International, West Conshohocken, PA, 1999.

[28] M. Jirásek and Z.P. Bažant. *Inelastic Analysis of Structures*. John Wiley & Sons, 2002.

[29] M. Klisinski. On constitutive equations for arbitrary stress-strain control in multi-surface plasticity. *Int J Solids Struct*, 35(20):2655–2678, 1998.

[30] J. Korelc. Multi-language and multi-environment generation of nonlinear finite element codes. *Eng Computers*, 18(4):312–327, 2002.

[31] E.H. Lee. Elasto-plastic deformation at finite strains. *J Appl Mech-ASME*, 36:1–6, 1969.

[32] J. Lemaitre. *A course on damage mechanics*. Springer, second edition, 1996.

[33] S. Li and A. Gupta. On dual configurational forces. *J. Elasticity*, 84(1):13–31, 2006.

[34] J. Lubliner. *Plasticity theory*. Macmillan, 1990.

[35] F. Ma, X. Deng, M.A. Sutton, and Jr. Newman, J.C. *Mixed-mode crack behavior*, chapter A CTOD-based mixed-mode fracture criterion, pages 86–110. Number STP 1359. ASTM American Society for Testing and Materials, West Conshohocken, PA, 1999.

[36] T.M. Maccagno and J.F. Knott. The mixed mode I/II fracture behavior of lightly tempered hy130 steel at room temperature. *Engineering Fracture Mechanics*, 41:805–820, 1992.

[37] J. Mandel. *Plasticité classique et viscoplasticité*. CISM Lecture Notes. Springer-Verlag, Udine, 1971.

[38] P. Mattila. *Geometry of sets and measures in Euclidean spaces-Fractals and rectifiability*. Cambridge studies in advanced mathematics. Cambridge, 1995.

[39] S. Nemat-Nasser. *Plasticity: A treatise on finite deformation of heterogeneous inelastic materials*. Cambrige University Press, 2004.

[40] J. Oliver. Continuum modelling of strong discontinuities in solid mechanics using damage models. *Comput Mech*, 17:49–61, 1995.

[41] Wolfram Research Inc. Mathematica, 2007.

[42] G. Rousselier, J.-C. Devaux, G. Mottet, and G. Devesa. *Nonlinear fracture mechanics: Volume II-Elastic-plastic fracture*, chapter "A methodology for ductile fracture analysis based on damage mechanics: an illustration of a local approach of fracture", pages 332–354. Number STP 995. American Society for Testing and Materials, Philadelphia, 1989.

[43] J.C. Simo. A framework for finite strain elastoplasticity based on maximum plastic dissipation and the multiplicative decomposition: Part I. continuum formulation. *Comp Method Appl M*, 66:199–219, 1988.

[44] J.C. Simo. A framework for finite strain elastoplasticity based on maximum plastic dissipation and the multiplicative decomposition: Part II. computational aspects. *Comp Method Appl M*, 68:1–31, 1988.

[45] J.C. Simo and T.J.R. Hughes. *Computational Inelasticity*. Interdisciplinary Applied Mathematics. Springer-Verlag, 1998.

[46] H.A. Sosa and J. Eischen. Computation of stress intensity factors for plate bending via a path-independent integral. *Engineering Fracture Mechanics*, 25(4):451–462, 1986.

[47] M. A. Sutton, X. Deng, J. C. Newman Jr. F. Ma, and M. James. Development and application of a crack tip opening displacement-based mixed mode fracture criterion. *International Journal of Solids and Structures*, 37:3591–3618, 2000.

[48] C. Truesdell and W. Noll. *The non-linear field theories of mechanics*. Springer, Third edition, 2004.

[49] N. Van Goethem, P. Areias, and E.B. Pires. A temperature-dependent damage model for ductile crack initiation and propagation with finite strains. In *CFRAC 2011 International Conference*, Barcelona, Spain, June 2011. CIMNE.

[50] N. Van Goethem and A. Novotny. Crack nucleation sensitivity analysis. *Math. Meth. Appl. Sc.*, 33(16), 2010.

[51] L. Xue and T. Wierzbicki. Ductile fracture initiation and propagation modeling using damage plasticity theory. *Eng. Fracture Mech.*, 75:3276–3293, 2008.